FEA Information
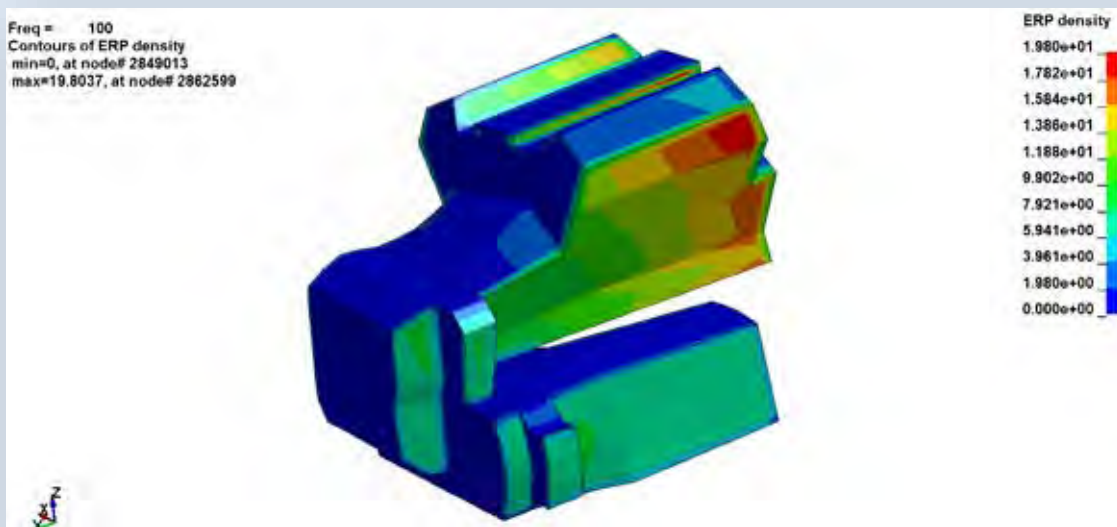# Engineering Journal

Article: Discussion on acoustic databases in LS-DYNA®.

FEA Information Engineering Journal

Aim and Scope

FEA Information Engineering Journal (FEAIEJ™) is a quarterly published online journal to cover the latest Finite Element Analysis Technologies.   The journal aims to cover previous noteworthy published papers and original development updates. All published papers are peer reviewed in the respective FEA engineering fields.

Consideration is given to all aspects of technically excellent written information without limitation on length.   All submissions must follow guidelines for publishing a paper, or periodical.   If a paper has been previously published, FEAIEJ requires written permission to reprint, with the proper acknowledgement give to the publisher of the published work.

Reproduction in whole, or part, without the express written permission of FEA Information Engineering Journal, or the owner of of the copyright work, is strictly prohibited.   FEAIJ welcomes unsolicited topics, ideas, and articles.

Monthly publication is limited to no more then five papers or informational articles of interest, either reprint, or original.

For information on publishing a paper original or reprint contact yanhua@feainformation.com Subject line: Journal Publication

Cover:

Fig. Figure 15. ERP density plot at frequency 100 Hz

Article: Discussion on acoustic databases in LS-DYNA

FEA Information Engineering Journal

TABLE OF CONTENTS

Publications are © to the authors and are informational publishings

A Customized Job Manager for Metal Forming Simulations

with LS-DYNA®

Yuzhong Xiao, Xinhai Zhu, Li Zhang, Houfu Fan
LSTC

Introduction

Generally the simulation time of the metal forming analysis is relatively short, but several numerical tryouts would be expected, due to the iterative modification of the forming tools based on the simulation results. Therefore it would be nice to provide a Graphic User Interface (GUI) for the user to manage the simulation jobs effectively (e.g. simplified submission procedures and quick file operations on the results), so that the total time cost could be further reduced. Also among various metal forming simulations, in addition to those with a single keyword file input, jobs that consist of several (e.g. the progressive die forming) or even dozens of sequential simulations (e.g. the iterative springback compensation process), are increasing. Based on these traits, a simple application (Job Manager) has been customized for our metal forming users with the intention to help them manage the simulation jobs.

Applications and settings of Job Manager

The submission of a multi-OP simulation

For multi-OP simulations like progressive die forming or springback compensation, the sequential submission of its OPs /stages is needed. And in most cases the precisions and the version of the solver would differ in different OPs. For example, the OP of implicit gravity or springback requires the double precision solver, while in the drawing and flanging simulations the single precision solver would be adequate but reduce the time cost. While new features are needed in trimming or springback compensation, official releases are still recommended for other common processes (e.g. drawing) because they are more stable.

Currently LS-PREPOST EZSetup has supported the setup of these jobs for metal forming users. The simulation of each OP will be performed in its own folder, making it clearer to process the results. A batch file will be created by LS-PREPOST EZSetup to perform the

simulations.   Now a GUI (Job manager) has been further customized with enhanced features for the users to manage the simulation jobs more easily.

The submission of a multi-OP job in Job Manager is shown in Fig. 1. The batch file created by LS-PREPOST EZsetup can be directly loaded into Job Manager. Automatic detection of the job status can help the user easily start or resume the workflow, without checking which of the OPs are already completed. In these multi-OP jobs, file cleaning is another time-consuming task for forming users, since a large number of files would be created in different folders. In Job Manager, a job file clean filter is preset and can be customized by the user to help clean all files that are no longer needed with one simple click.
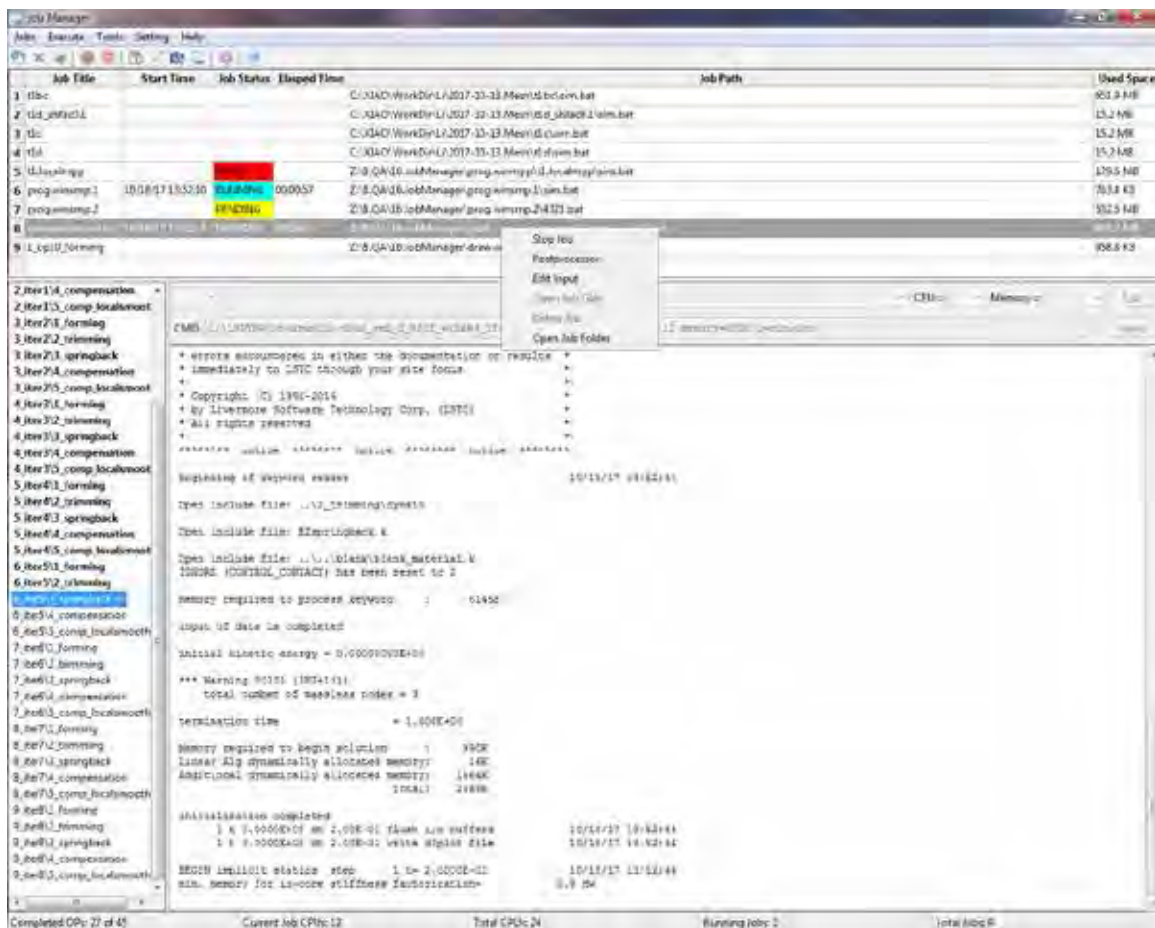

Fig.1 Multi-OP submission from the EZsetup batch file in Job Manager

The submission of a single process simulation

A common single submission (e.g. a single drawing simulation or the blank shape estimation with the one step method) is also supported by Job Manager. The solution

settings allow the user to select the preset default solvers, CPU and memory parameters, or directly browse for another solver and input the solution parameters manually, as shown in Fig.2.
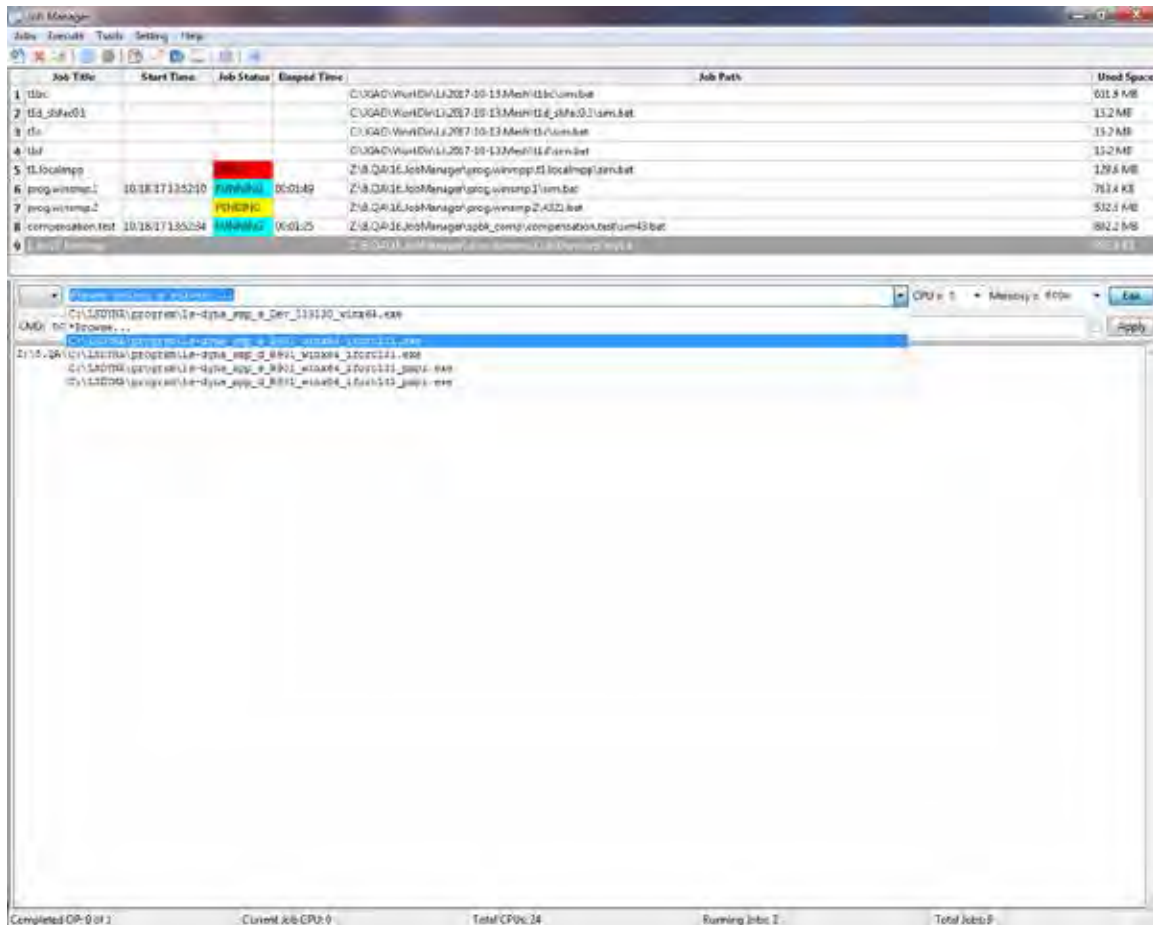

Fig. 2 Single submission of a single keyword inputdeck in Job Manager

The user settings in Job Manager

As shown in Fig.3, the user settings can be defined and saved in the configuration window.

The default parameter for the SMP and MPP solvers can be specified and become available in the solver lists as in Fig.2. Besides using local solvers, the submission commands can also be customized here according to the user's job submission protocol (currently working with Windows OS). So it is possible to run different OPs of the same job in the local workstation and HPC in a mixed manner (e.g. simulating forming in the HPC for the faster and stable solution with the official release, and then spring-back

compensation in the local workstation for the new features in a beta solver). The license setup let the user run LSDYNA with valid license info, without modifying the system environment variables (this is useful when the user has valid license info but no administrative privilege). It also allows the user to define the postprocessor, the text editor and the job file clean filter for quick file operations from the toolbar or the popup menus in the main window.
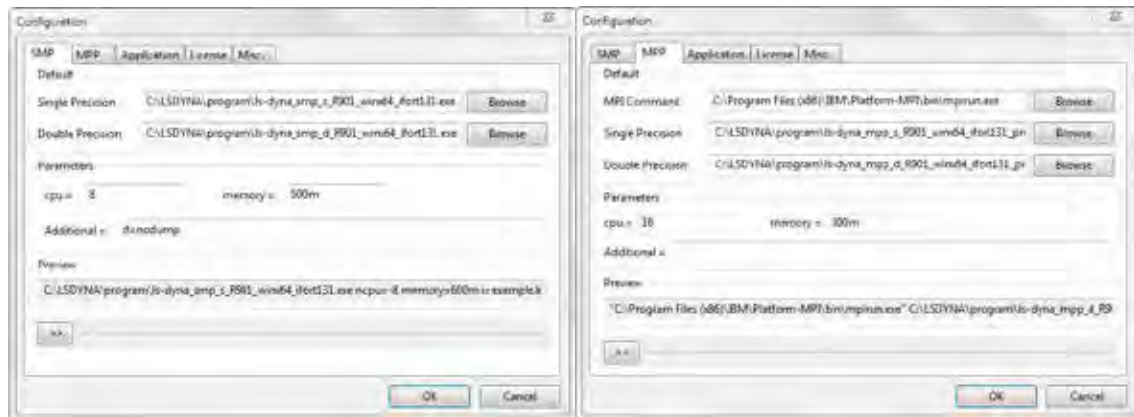

Fig. 3 the user settings in Job Manager

Current features of Job Manager

1. Supporting sequential submission of the multi-OP jobs in metal forming simulations (e.g. progressive die simulation) minimizes the possible waiting time between two OPs to reduce the total time cost.
2. Automatic multi-OP job status detection makes it easier for the user to resume the job correctly and prevent the possible file conflict in case of running tests in the same folder. Nevertheless the user can still start from a specified OP via the pop-up menu.
3. Two ways are implemented to add a job:
    a) via GUI: the Windows batch file from EZSetup in LS-PREPOST or the LS-DYNA keyword file can be loaded by using "Add job" button or directly dragging the file into Job Manager;
    b) via command line: parameters can be passed to Job Manager so that the job can be added, started and deleted by a preprocessor (tested with an alpha version of LS-FORM).
4. The local SMP and MPP solvers are supported. It also works with the HPC that supports Windows submission command (tested with HPC of GM).
5. Real-time update of the solver message for the running job (local) allows the user to easily monitor the simulation progress.

6. The solver info can be loaded from the EZSetup file or manually defined, allowing the user to change the solver settings for a partially completed multi-OP job.

7. A fail-safe scheme is implement to instantly restore the work flow of running jobs upon staring Job Manager, in case of abnormal termination of Job Manger (crashed or terminated in OS for a update) .The current Windows batch has the limitation that the user would have to wait for the current OP to finish or kill it to restart the batch file in order to resume the process monitoring.

8. Utilities such as the popup menus, job grid sorting, simulation files cleaning and hard disk usage make it easier to manage the simulations (especially jobs consisting of dozens of OPs like springback compensation).

9. As a standalone executable, it allows the user to close the pre-processor after submitting the job. The user-defined shortcut to launch the post-processor also helps the user to quickly evaluate the results.

Summary

A user-friendly GUI has been customized for LSDYNA metal forming users, with the intention to help them manage the simulation jobs effectively and further reduce total time cost. The current version works in MS Windows. The future vision may also be extended to Linux.

Acknowledgement

Important help and valuable feedbacks from LSTC LSPP team are greatly appreciated. Special thanks go to General Motors Corporation for HPC tests.

Thick Shell Element Form 5 in LS-DYNA

Lee P. Bindeman
Livermore Software Technology Corporation

Thick shell form 5 in LS-DYNA is a layered 8 node brick element, with 4 nodes defining the bottom surface and 4 defining the top. For computational efficiency, each layer has one in-plane integration point. At least 2 layers are needed through the thickness, but there is no limit to the number of layers that may be defined.
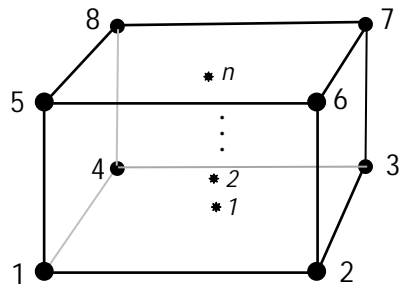

Fig. 1.1 Thick shell element form 5 with n integration points.

The through-thickness orientation of the integration points gives the element the ability to capture bending like a plate or shell element, but it can also capture the thickness stress like a brick element. Like brick element form 1, thick shell form 5 is based on the trilinear shape functions.

Before describing how the strain is evaluated, it is useful to introduce two coordinate systems, one being a corotational system $(\hat{x}, \hat{y}, \hat{z})$, and the second a referential coordinates system (x, h, z). The map to the corotational system is a simple rotation from the global coordinate system. The corotational system has its origin at the element centroid, and is defined by vectors that pass through the centers of opposite faces. For skewed elements, the corotational system is orthogonalized and may not pass exactly through face centers. In the referential system, the element is a cube with edge lengths of 2. The origin of the referential system is at the center and the axes intersect the element faces at -1 and
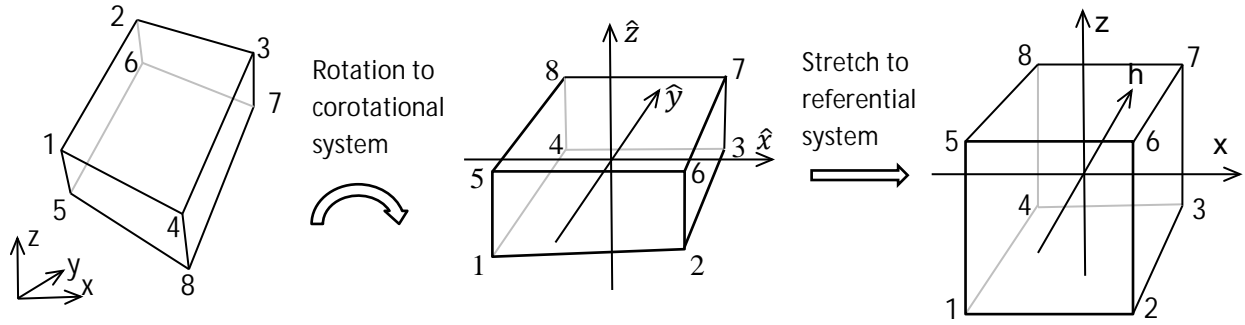
+1.

Fig. 1.2 Element geometry in global, corotational, and referential coordinate systems

In the referential system, we can evaluate a variable at any location within the element in terms of nodal values, u_I, using the trilinear shape functions as shown in Eq. 1.1.

$$u(\xi,\eta,\zeta) = N_I(\xi,\eta,\zeta)u_I \qquad\qquad \text{Eq. 1.1}$$

In Eq. 1.1 and those that follow, the upper case subscript, I, refers to node numbers 1 to 8, and the repeated subscript indicates a summation from 1 to 8. Below, lower case subscripts will refer to the spatial coordinates, 1 to 3. The well-known trilinear shape functions can be written at each node in terms of the referential coordinates, and the value of the referential coordinates at the node, either +1 or -1.

$$N_I(\xi,\eta,\zeta) = \frac{1}{8}(1 + \xi_I\xi)(1 + \eta_I\eta)(1 + \zeta_I\zeta) \qquad\qquad \textbf{Eq. 1.2}$$

The development of a strain field follows the development for the 1-point brick element in Belytschko and Bindeman, 1993, where it was shown that the displacement or velocity field could be written in terms of the shape function derivatives, b, orthogonal gamma vectors of Belytschko, Ong, Liu, and Kennedy, 1984, and the nodal values of displacements or velocities, v_i.

$$v_i = a_{0i} + \left(xb_x^t + yb_y^t + zb_z^t + h_1\gamma_1^t + h_2\gamma_2^t + h_3\gamma_3^t + h_4\gamma_4^t\right)v_i \qquad\qquad \text{Eq. 1.3}$$

$$\widehat{b}_x^t = \frac{1}{V}\int_{\Omega_e}\frac{\partial N(\xi,\eta,\zeta)}{\partial x}d\Omega \qquad\qquad \text{Eq. 1.4}$$

$$\widehat{\gamma}_\alpha = \frac{1}{8}\left[h_\alpha - \sum_{j=1}^{3}\left(h_\alpha^t x_j\right)\widehat{b}_j\right] \qquad\qquad \text{Eq. 1.5}$$

In Eq. 1.3, h_1 to h_4 are defined in terms of the referential coordinates.

$$h_1 \equiv \eta\zeta \qquad h_2 \equiv \zeta\xi \qquad h_3 \equiv \xi\eta \qquad h_4 \equiv \xi\eta\zeta \qquad\qquad \text{Eq. 1.6}$$

In Eq. 1.4, the integral is over the element domain, and closed form expressions are in terms of nodal coordinates are presented in Belytschko et al., 1984. In Eq. 1.7, the expressions for h_1 to h_4 have been evaluated at the 8 nodes to create 8x1 arrays of +1 and -1.

$$
\begin{aligned}
\boldsymbol{h}_1^t &\equiv (+1, +1, -1, -1, -1, -1, +1, +1) \\
\boldsymbol{h}_2^t &\equiv (+1, -1, -1, +1, -1, +1, +1, -1) \\
\boldsymbol{h}_3^t &\equiv (+1, -1, +1, -1, +1, -1, +1, -1) \\
\boldsymbol{h}_4^t &\equiv (-1, +1, -1, +1, +1, -1, +1, -1)
\end{aligned}
$$

Eq. 1.7

Using Eq. 1.3 with nodal velocities, $\boldsymbol{v}_I$, and taking the derivative with respect to the corotational coordinates, we get terms of the spatial gradient of velocity, $\boldsymbol{L}$.

$$
L_{ij} = \frac{\partial v_i}{\partial \hat{x}_j} = \sum_{I=1}^{8} \frac{\partial N_I}{\partial x_j} v_{iI} = \left(\widehat{\boldsymbol{b}}_j^t + h_{\alpha,j}\widehat{\boldsymbol{\gamma}}_\alpha^t\right) v_i
$$

Eq. 1.8

The strain measure of the element will be calculated from the rate-of-deformation, $\boldsymbol{D}$ which is the symmetric part of $\boldsymbol{L}$. If the 6 unique terms of the rate-of-deformation are arranged in a 6x1 array, then the calculation of them can be written as a matrix multiplication.

$$
\begin{Bmatrix} D_{11} \\ D_{22} \\ D_{33} \\ D_{12} \\ D_{13} \\ D_{23} \end{Bmatrix} =
\begin{bmatrix}
\widehat{\boldsymbol{b}}_x^t + h_{\alpha,x}\widehat{\boldsymbol{\gamma}}_\alpha^t & 0 & 0 \\
0 & \widehat{\boldsymbol{b}}_y^t + h_{\alpha,y}\widehat{\boldsymbol{\gamma}}_\alpha^t & 0 \\
0 & 0 & \widehat{\boldsymbol{b}}_z^t + h_{\alpha,z}\widehat{\boldsymbol{\gamma}}_\alpha^t \\
\widehat{\boldsymbol{b}}_y^t + h_{\alpha,y}\widehat{\boldsymbol{\gamma}}_\alpha^t & \widehat{\boldsymbol{b}}_x^t + h_{\alpha,x}\widehat{\boldsymbol{\gamma}}_\alpha^t & 0 \\
\widehat{\boldsymbol{b}}_z^t + h_{\alpha,z}\widehat{\boldsymbol{\gamma}}_\alpha^t & 0 & \widehat{\boldsymbol{b}}_x^t + h_{\alpha,x}\widehat{\boldsymbol{\gamma}}_\alpha^t \\
0 & \widehat{\boldsymbol{b}}_z^t + h_{\alpha,z}\widehat{\boldsymbol{\gamma}}_\alpha^t & \widehat{\boldsymbol{b}}_y^t + h_{\alpha,y}\widehat{\boldsymbol{\gamma}}_\alpha^t
\end{bmatrix}
\cdot \begin{Bmatrix} v_x \\ v_y \\ v_z \end{Bmatrix}
$$

Eq. 1.9

Eq. 1.9, $\boldsymbol{b}_i^t$ and $\boldsymbol{\gamma}_x^t$ are 1x8 arrays of nodal values, and $\boldsymbol{v}_i$ is a 8x1 array of nodal velocities. The repeated alpha subscripts on h and $\boldsymbol{g}$ indicate a summation from 1 to 4. Calling the matrix with the $\boldsymbol{b}_i^t$ and $\boldsymbol{\gamma}_x^t$ terms $\boldsymbol{B}$, we can write the Eq. 1.9 as a matrix multiplication.

$$
\boldsymbol{D} = \boldsymbol{B} \cdot \boldsymbol{v}
$$

Eq. 1.10

To be correct, the bottom 3 rows of $\boldsymbol{B}$ should be scaled by ½, but omitting this should not cause confusion and simplifies the equations.

Eq. 1.9 is gives the rate of deformation that is consistent with the trilinear shape functions. If this was used as a strain measure for the element, it would exhibit volumetric locking and excessive shear stiffness. Modifications to the B matrix were made in Belytschko and Bindeman, 1993, to correct these problems in a 1-point brick based on the QBI assumed strain field where QBI is an acronym for quintessential bending incompressible. Thick shell form 5 also uses the QBI assumptions, not only for hourglass control, but also to modify the strain rate at the integration points to achieve element stress with the same beneficial properties. Because thick shell form 5 is a layered element, it can achieve accurate coarse mesh results with nonlinear material models as well as the linear solutions that the brick can achieve.

To prevent locking in incompressible materials, the QBI strain field adds terms in the upper half of the matrix to approximate Poisson's effects. It also removes terms from the bottom half to prevent excessive shear stiffness during bending. This shear correction is consistent with assuming the top and

bottom surface of the element is curved during bending so that there is no shear stress during pure bending.

To simplify equations, we introduce notation with up to four subscripts that indicate which terms of the summation are retained, and X, Y, or Z is used to indicate the variable for the partial derivative. Examples of this notation are shown in Eqs. 1.11.

$$\widehat{X}_{1234} \equiv \sum_{\alpha=1}^{4} h_{\alpha,x} \widehat{\gamma}_{\alpha}^{t} \qquad \widehat{Y}_{1234} \equiv \sum_{\alpha=1}^{4} h_{\alpha,y} \widehat{\gamma}_{\alpha}^{t} \qquad \widehat{Z}_{1234} \equiv \sum_{\alpha=1}^{4} h_{\alpha,z} \widehat{\gamma}_{\alpha}^{t} \qquad \text{Eq. 1.11}$$

$$\widehat{X}_{14} \equiv h_{1,x} \widehat{\gamma}_{1}^{t} + h_{4,x} \widehat{\gamma}_{4}^{t} \qquad \widehat{Y}_{12} \equiv h_{1,y} \widehat{\gamma}_{1}^{t} + h_{2,y} \widehat{\gamma}_{2}^{t}$$

Using Eqs. 1.10, the B matrix for the QBI assumed strain is shown in Eq. 1.11.

$$B = \begin{bmatrix} \widehat{b}_{x}^{t} + \widehat{X}_{1234}^{t} & -\bar{v}\widehat{Y}_{3}^{t} - v\widehat{Y}_{24}^{t} & -\bar{v}\widehat{Z}_{2}^{t} - v\widehat{Z}_{34}^{t} \\ -\bar{v}\widehat{X}_{3}^{t} - v\widehat{X}_{14}^{t} & \widehat{b}_{y}^{t} + \widehat{Y}_{1234}^{t} & -\bar{v}\widehat{Z}_{1}^{t} - v\widehat{Z}_{34}^{t} \\ -\bar{v}\widehat{X}_{2}^{t} - v\widehat{X}_{14}^{t} & -\bar{v}\widehat{Y}_{1}^{t} - v\widehat{Y}_{24}^{t} & \widehat{b}_{z}^{t} + \widehat{Z}_{1234}^{t} \\ \widehat{b}_{y}^{t} + \widehat{Y}_{12}^{t} & \widehat{b}_{x}^{t} + \widehat{X}_{12}^{t} & 0 \\ \widehat{b}_{z}^{t} + \widehat{Z}_{13}^{t} & 0 & \widehat{b}_{x}^{t} + \widehat{X}_{13}^{t} \\ 0 & \widehat{b}_{z}^{t} + \widehat{Z}_{23}^{t} & \widehat{b}_{y}^{t} + \widehat{Y}_{23}^{t} \end{bmatrix} \qquad \text{Eq. 1.12}$$

Because the corotational coordinate system and the referential coordinate system area aligned, we can make the simplifying assumptions in Eq. 1.13. For skewed elements, Eqs. 1.13 are only approximate, but Belytschko and Bindeman, 1993, concluded that the assumptions do not affect element behavior.

$$\frac{\partial \xi_{i}}{\partial \widehat{x}_{i}} = \frac{1}{\partial \widehat{x}_{i} / \partial \xi_{i}} = \frac{1}{\frac{1}{8}(\Lambda_{i}^{t} \widehat{x}_{i})} \qquad \frac{\partial \xi_{i}}{\partial \widehat{x}_{j}} = 0 \text{ for } i \neq j \qquad \text{Eq. 1.13}$$

In Eq. 1.13, the Λ terms are 8x1 arrays of +1 and -1 what that represent the stretching modes in the referential system.

$$\Lambda_{1}^{t} \equiv (-1, +1, +1, -1, -1, +1, +1, -1)$$

$$\Lambda_{2}^{t} \equiv (-1, -1, +1, +1, -1, -1, +1, +1)$$

$$\Lambda_{3}^{t} \equiv (-1, -1, -1, -1, +1, +1, +1, +1)$$

With Eq. 1.13, and the fact that $\xi=0$ and $\eta = 0$ for all integration points, we can consider the partial derivatives of h_1 to h_4 from Eq. 1.6. There are some terms that will be zero throughout the element domain because the partial derivatives are everywhere zero. Others will be non-zero throughout most of the element domain. A third type will be zero at the integration points, but nonzero elsewhere in the element domain. Examples of the 3 types are shown in Eqs. 1.15 to 1.17.

$$\frac{\partial h_1}{\partial x} = \frac{\partial \eta}{\partial x} \zeta + \eta \frac{\partial \zeta}{\partial x} = 0 \text{ everywhere} \qquad \text{Eq. 1.15}$$

$$\frac{\partial h_1}{\partial y} = \frac{\partial \eta}{\partial y} \zeta + \eta \frac{\partial \zeta}{\partial y} \neq 0 \text{ everywhere except } \zeta = 0 \qquad \text{Eq. 1.16}$$

$$\frac{\partial h_1}{\partial z} = \frac{\partial \eta}{\partial z}\zeta + \eta \frac{\partial \zeta}{\partial z} = 0 \text{ at integration points but nonzero where } \eta \neq 0 \qquad \text{Eq. 1.17}$$

We can omit the first type from $\boldsymbol{B}$ because they do not contribute anything. The second type will be included in the calculation of strain. The third type will used in the hourglass control. We can then split $\boldsymbol{B}$ into 2 parts, $\overline{\boldsymbol{B}}$ which will generate strain at the integration points and is passed to the stress update routine, and $\widetilde{\boldsymbol{B}}$ which will be used to construct hourglass control.

$$\boldsymbol{B} = \overline{\boldsymbol{B}} + \widetilde{\boldsymbol{B}} \qquad\qquad \textbf{Eq. 1.18}$$

$$\overline{\boldsymbol{B}} = \begin{bmatrix} \widehat{\boldsymbol{b}}_x^t + \widehat{\boldsymbol{X}}_2^t & \boldsymbol{0} & \boldsymbol{0} \\ \boldsymbol{0} & \widehat{\boldsymbol{b}}_y^t + \widehat{\boldsymbol{Y}}_1^t & \boldsymbol{0} \\ -\bar{v}\widehat{\boldsymbol{X}}_2^t & -\bar{v}\widehat{\boldsymbol{Y}}_1^t & \widehat{\boldsymbol{b}}_z^t \\ \widehat{\boldsymbol{b}}_y^t + \widehat{\boldsymbol{Y}}_1^t & \widehat{\boldsymbol{b}}_x^t + \widehat{\boldsymbol{X}}_2^t & \boldsymbol{0} \\ \widehat{\boldsymbol{b}}_z^t & \boldsymbol{0} & \widehat{\boldsymbol{b}}_x^t \\ \boldsymbol{0} & \widehat{\boldsymbol{b}}_z^t & \widehat{\boldsymbol{b}}_y^t \end{bmatrix} \qquad \text{Eq. 1.19}$$

$$\widetilde{\boldsymbol{B}} = \begin{bmatrix} \widehat{\boldsymbol{X}}_{34}^t & -\bar{v}\widehat{\boldsymbol{Y}}_3^t - v\widehat{\boldsymbol{Y}}_4^t & -\bar{v}\widehat{\boldsymbol{Z}}_2^t - v\widehat{\boldsymbol{Z}}_4^t \\ -\bar{v}\widehat{\boldsymbol{X}}_3^t - v\widehat{\boldsymbol{X}}_4^t & \widehat{\boldsymbol{Y}}_{34}^t & -\bar{v}\widehat{\boldsymbol{Z}}_1^t - v\widehat{\boldsymbol{Z}}_4^t \\ -v\widehat{\boldsymbol{X}}_4^t & -v\widehat{\boldsymbol{Y}}_4^t & \widehat{\boldsymbol{Z}}_{124}^t \\ \boldsymbol{0} & \boldsymbol{0} & \boldsymbol{0} \\ \widehat{\boldsymbol{Z}}_1^t & \boldsymbol{0} & \widehat{\boldsymbol{X}}_3^t \\ \boldsymbol{0} & \widehat{\boldsymbol{Z}}_2^t & \widehat{\boldsymbol{Y}}_3^t \end{bmatrix} \qquad \text{Eq. 1.20}$$

With $\overline{\boldsymbol{B}}$ we can evaluate the rate-of-deformation at the integration points which can be used to incrementally update the stress to generate nodal forces, as shown in Eq. 1.21.

$$\boldsymbol{D} = \overline{\boldsymbol{B}} \cdot \boldsymbol{v}$$

$$\sigma^n = \sigma^{(n-1)} + f(\boldsymbol{C}, \boldsymbol{D}\Delta t, h) \qquad \text{Eq. 1.21}$$

$$\overline{\boldsymbol{f}}^n = \int_{\Omega_e} \overline{\boldsymbol{B}}^t \cdot \sigma^n \, d\Omega$$

If needed, we can also construct an element stiffness matrix.

$$K = \int_{\Omega_e} \overline{\boldsymbol{B}}^t \cdot \boldsymbol{C} \cdot \overline{\boldsymbol{B}} \, d\Omega \qquad \text{Eq. 1.22}$$

In Eq. 1.21, the superscripts $n-1$ and n indicate sequential solution time steps. The function f represents the stress update routine and is a function of the constitutive properties, $\boldsymbol{C}$, the current deformation, and possibly history variables, h. Integration in Eq. 1.21 and Eq. 1.22 is over the element domain, Ω_e. It is done by evaluating the terms within the integral at the integration points, and using appropriate numerical integration factors.

Similarly, with $\widetilde{\boldsymbol{B}}$, we can update hourglass forces and construct an hourglass stiffness if needed. The procedure is similar to Eq. 1.21 and 1.22.

$$\boldsymbol{h} = \widetilde{\boldsymbol{B}} \cdot \boldsymbol{v}$$

$$\boldsymbol{H}^n = \boldsymbol{H}^{(n-1)} + \boldsymbol{C_h} \cdot \boldsymbol{h}\Delta t \qquad\qquad\qquad\qquad\qquad \text{Eq. 1.23}$$

$$\widetilde{\boldsymbol{f}}^n = \int_{\Omega_e} \widetilde{\boldsymbol{B}}^t \cdot \boldsymbol{H}^n \, d\Omega$$

Instead of evaluating $\boldsymbol{D}$ and $\boldsymbol{\sigma}$ as in Eq. 1.21, we have intermediate terms $\boldsymbol{h}$ and $\boldsymbol{H}$ in Eq. 1.23 which could be called the hourglass deformation rate and hourglass stress. $\boldsymbol{H}$ is a function of material properties, $\boldsymbol{C_h}$ which for many materials are the elastic constitutive matrix, but for plasticity models, the average tangent modulus is used. The use of elastic constants is usually sufficiently accurate as the energy in the hourglass mode of the thick shell is typically very small compared to the strain energy, particularly because the modes for bending about the $\hat{x}$ axis and $\hat{y}$ axis are included in the stress update. Therefore, plate bending with thick shells does not require stacking elements as it does with bricks. The integration in Eq. 1.23 is done in closed form so no looping over integration points is needed.

The D_{13} and D_{23} terms of rate-of-deformation calculated by 1.21 are the same at all integration points. It is well know that for a rectangular cross section, the out-of-plane shear stress will have a parabolic distribution with maximum stress at the mid-plane and zero stress at the outer surfaces. To achieve this, D_{13} and D_{23} are scaled for each layer. The scale factors will be continuously recalculated for plasticity models such that proper shear distribution will be maintained as layers of the element reach the yield surface of the material. The parabolic stress may be inappropriate if elements are stacked one on top of the other, so the user may choose a constant distribution. If neither distribution is appropriate, the user may define a scale factor for each layer to achieve a desired shear distribution.

To this point, the discussion has assumed that the material is homogenous. In other words, all layers use the same material model with the same properties. For modeling layered composites of fiber reinforced materials, the strong fiber direction may vary by layer. Other composite models may use different materials or material properties in different layers. For modeling composites, the options described above for scaling D_{13} and D_{23} are unlikely to work well because the relationship between stress and strain is no longer consistent between layers. To account for layers of varying stiffness, an additional scaling of D_{13} and D_{23} is done such that the shear stress distribution is either parabolic, constant, or user-defined.

Similarly, the constant assumption for the D_{33} term may not be accurate for composite models. Therefore, a correction is made to the through-thickness strain to approximate a constant through-thickness stress distribution. With this correction, soft layers will have larger strain increments than stiff layers. This correction may not only improve the solution in the thickness direction, but may also improve the in-plane stress due to Poisson's effects.

These modifications to D for nonhomogeneous materials enable thick shell 5 to capture some of the complexity in the behavior of layered composites. The use of reduced integration within the layers enables fast explicit solutions.

Thick shell 6 is nearly identical to thick shell 5. However, instead of using full 3-D stress updates, it uses plane stress updates that are used by the thin shell elements. An uncoupled z-stress is added to the 2D stress such that there will be reasonable energy for deformation in the thickness direction. Thick shell 6 is therefore most appropriate where a plane-stress assumption is reasonable. The library of available material models for the thin shells differs to the 3D library, so the availability of a desired material model might dictate which element is used.

References

Belytschko, T. and Bindeman, L. P. "Assumed Strain Stabilization of the Eight Node Hexahedral Element," Comp. Meth. Appl. Mech. Eng. 105, 225-260 (1993).

Belytschko, T., Ong J. S.,-J., Liu, W. K., and Kennedy, J. M. "Hourglass Control in Linear and Nonlinear Problems," Comp. Meth. Appl. Mech. Eng. 43, 251-276 (1984).

Discussion on acoustic databases in LS-DYNA^Ò

Zhe Cui, Yun Huang

Livermore Software Technology Corporation

Abstract: A bunch of acoustic solvers have been provided by LS-DYNA. They include the ones based on boundary element methods (keyword ***FREQUENCY_DOMAIN_ACOUSTIC_BEM**, including the approximate methods: Rayleigh method, Kirchhoff method), finite element methods (keyword ***FREQUENCY_DOMAIN_ACOUSTIC_FEM**, and vibration solvers (ERP, equivalent radiated power, based on Steady State Dynamics, keyword ***FREQUENCY_DOMAIN_SSD_ERP**).

The acoustic solvers have been widely used in NVH, vibro-acoustic analysis and many other areas where noise level or sound quality is a concern. To perform the post-processing of the acoustic analysis with LS-DYNA, a bunch of databases have been implemented.

For fringe plot of the results, the following binary databases have been provided: D3ACS, D3ACP, D3ACC, D3ATV, D3ERP and D3EIGV_AC;

For xyplot of the results, the following ASCII databases have been provided: Press_Pa, Press_dB, Press_Pa_real, Press_Pa_imag, Press_Pa_t, Press_dB_t, Press_Power, Press_radef, Press_dB(A), Press_dB(B), Press_dB(C), Press_dB(D) and panel_contribution_NID.

These databases have different purposes and should be used under different circumstances.

1. Introduction

Since ls971 R6 version, a series of frequency domain features of acoustic simulation have been implemented to LS-DYNA. They include the ones based on boundary element methods (keyword ***FREQUENCY_DOMAIN_ACOUSTIC_BEM**, including the approximate methods: Rayleigh method, Kirchhoff method), finite element methods (keyword ***FREQUENCY_DOMAIN_ACOUSTIC_FEM**) and vibration solvers (ERP, equivalent radiated power, based on Steady State Dynamics, keyword ***FREQUENCY_DOMAIN_SSD_ERP**). They were developed to meet requirements from users of different industries, especially those from auto NVH analysis.

A bunch of databases have been provided for the post-processing of the acoustic analysis with LS-DYNA. All these database files can be accessed by LS-PrePost. This paper gives a brief review of these databases.

2. Binary database for fringe plot

2.1 D3ACS

The binary plot file D3ACS shows the solution of frequency domain FEM acoustic computation or collocation BEM acoustic computation. The acoustic computation is activated by the keyword ***FREQUENCY_DOMAIN_ACOUSTIC_FEM** or ***FREQUENCY_DOMAIN_ACOUSTIC_BEM**.

The solution of FEM or collocation BEM acoustic computation is given as complex acoustic pressure on the nodes. For FEM acoustic analysis, the user gets the acoustic pressure in the finite element acoustic volume (including the surface); for collocation BEM acoustic analysis, the user gets the acoustic pressure on the

surface (boundary elements) of the acoustic volume. The real and imaginary parts of the pressure, the magnitude of the pressure, the sound pressure level (dB), and the normal velocity on the surface nodes are provided in D3ACS as nodal state variables for each output frequency. For collocation BEM, the acoustic intensity ($\frac{1}{2}\mathrm{Re}\{pv^*\}$)) is computed based on acoustic pressure p and normal velocity v, and is also output to D3ACS.

A cylinder model is adopted to illustrate the D3ACS database for acoustic BEM solver (figure 1). For simplicity, the cylinder is assumed to be subjected to uniform normal velocity for the whole range of frequency. Figure 2 shows the contour of sound pressure level at frequency 211.92 Hz, which is from D3ACS file.

uniform normal velocity
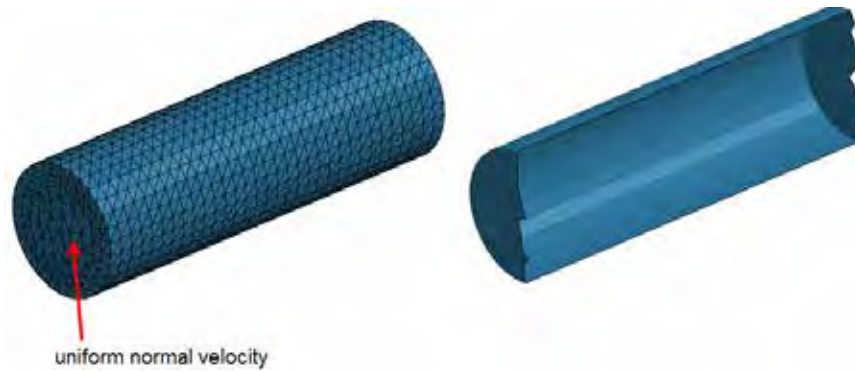
Figure 1. A cylinder BEM model
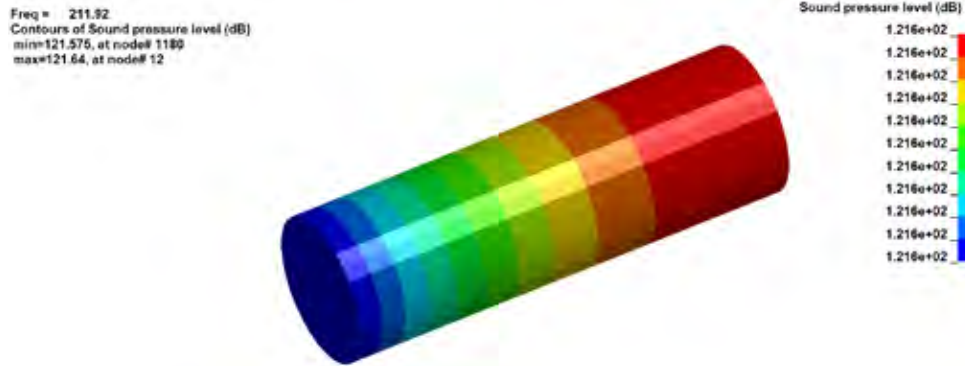
Figure 2. Sound pressure Level (dB) at frequency 211.92 Hz

Uniform normal velocity
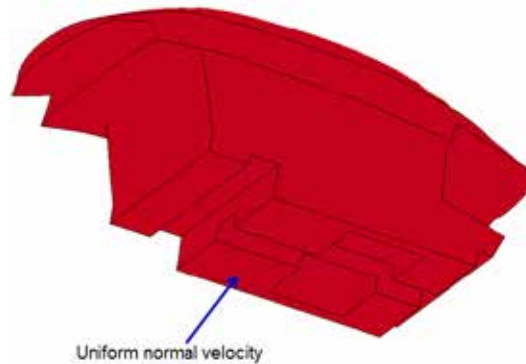
Figure 3. Simple compartment FEM model

A simple compartment model is used to illustrate the D3ACS database for acoustic FEM solver (figure 3). For simplicity, the compartment is assumed to be subjected to uniform normal velocity at the base for the whole range of frequency. Figures 4a and 4b show the contour of magnitude of sound pressure on the surface and in the acoustic volume at frequency 10 Hz, given by D3ACS file. One can see that the BEM solver gets the acoustic pressure on the surface, while the FEM solver gets acoustic pressure in the acoustic volume as well as on the surface.
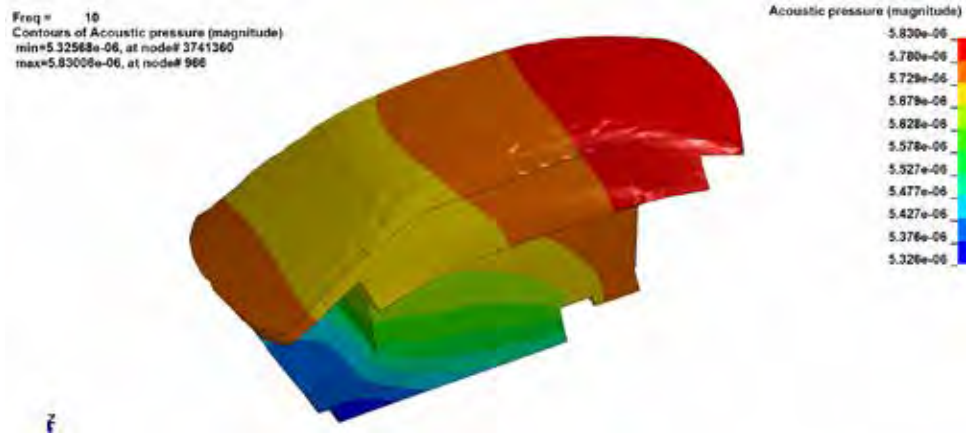
Figure 4a. Sound pressures (magnitude) on the surface at frequency 10 Hz
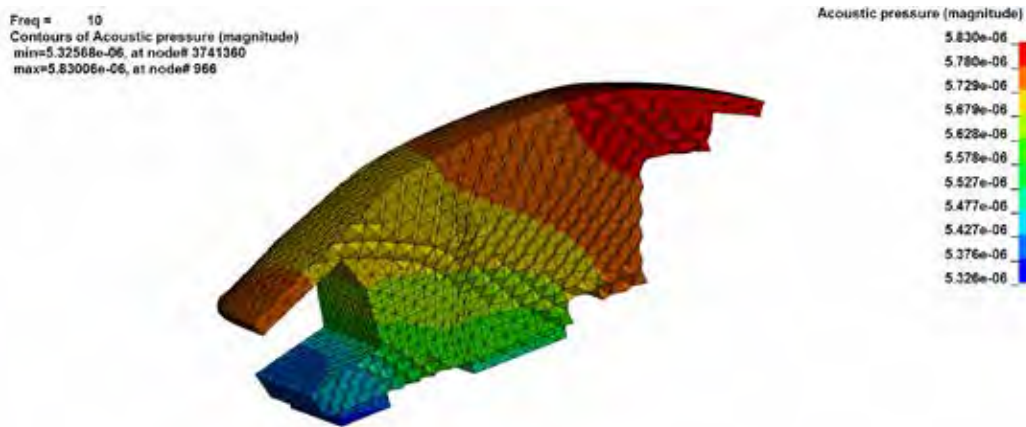
Figure 4b. Sound pressures (magnitude) in the acoustic volume at frequency 10 Hz

2.2 D3ACP

The binary plot file D3ACP shows the fringe plot of acoustic pressure at field points in BEM acoustic analysis. The field points are defined by the keyword ***FREQUENCY_DOMAIN_ACOUSTIC_FRINGE_PLOT**.

The results of acoustic analysis are given as complex acoustic pressure at the field points. The real and imaginary parts of the pressure, acoustic intensity, the magnitude of the pressure and the sound pressure level (dB) are written to D3ACP as nodal state variables for each output frequency. Acoustic intensity is computed by assuming a plane wave condition, as shown in equation (1).

$$I = \frac{1}{2}\,\mathrm{Re}\{pv_n^*\} = \frac{1}{2}\,\mathrm{Re}\left\{p\frac{p^*}{rc}\right\} = \frac{1}{2rc}\,\mathrm{Re}\{pp^*\} \tag{1}$$

Where p is the acoustic pressure (p^* is the conjugate of p), r is the density of acoustic medium, c is the sound speed and v_n is the normal velocity on the surface of the structure.

A simple car model is used to illustrate the D3ACP database. Figure 5 is the simple car model. Figure 6 shows the real and imaginary parts of the acoustic pressure contour at 71Hz.
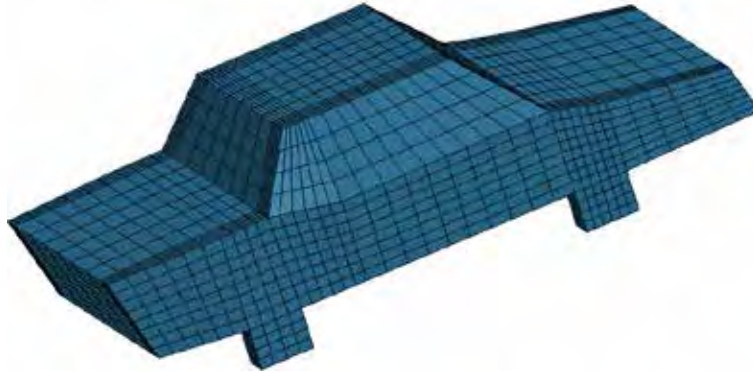

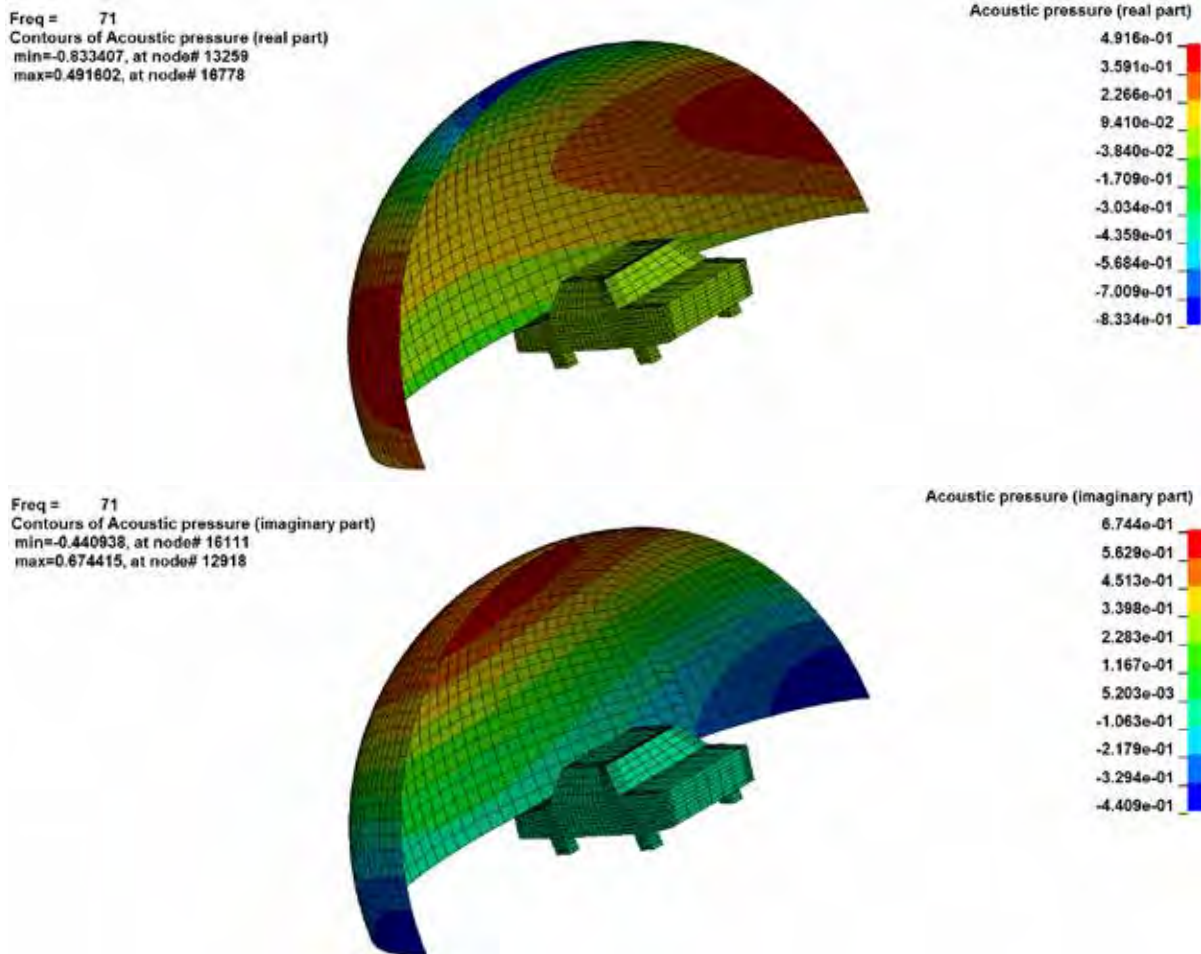Figure 5. A simple car BEM model

Figure 6. Real and imaginary parts of sound pressures at frequency 71 Hz

2.3 D3ACC

The binary plot file D3ACC saves element acoustic pressure contribution and contribution percentage on selected field points from a boundary element acoustic analysis. The acoustic analysis is activated by the keyword ***FREQUENCY_DOMAIN_ACOUSTIC_BEM**. The dump of this file is activated by the keyword ***DATABASE_FREQUENCY_BINARY_D3ACC**.

The idea of this contribution analysis is that according to equation (2), the acoustic pressure p at a field point P is given as a combination of the pressure p_j contributed by each of the boundary elements.

$$p(P) = \sum_{j=1}^{N} \int_{G_j} \left(G \frac{\partial p}{\partial n} - p \frac{\partial G}{\partial n} \right) dG_j = \sum_{j=1}^{N} p_j(P) \tag{2}$$

In equation (2), G is the acoustic fundamental solution in free space and n is the normal direction of the boundary elements.

To compute the contribution percentage of an element to the acoustic pressure at a field point, vector projection like the one shown in figure 7 is used. This is because the acoustic pressure, in frequency domain, is given as complex variables.
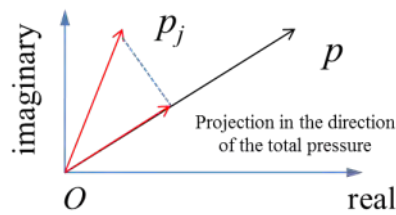

Figure 7. Computation of contribution percentage using vector projection

A simple car compartment model is used to illustrate the D3ACC database (figure 8). Figure 9 shows the real part of the element acoustic pressure contribution towards field point 100001 at frequency 300 Hz. Figure 10 shows the element contribution percentage for acoustic pressure at field point 100001 at 300 Hz. Please note, the element acoustic pressure contribution (and contribution percentage) not only vary with frequency, but also vary with field points.
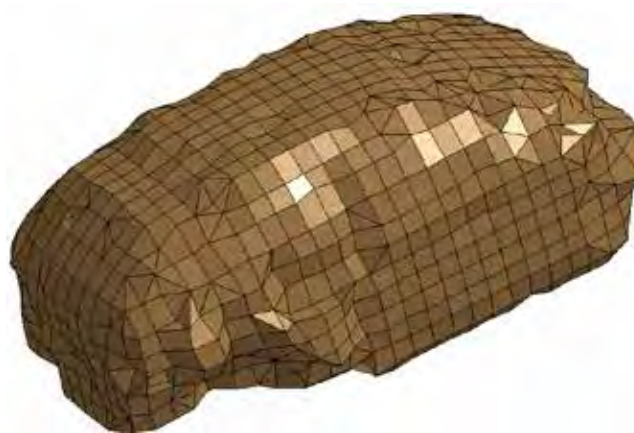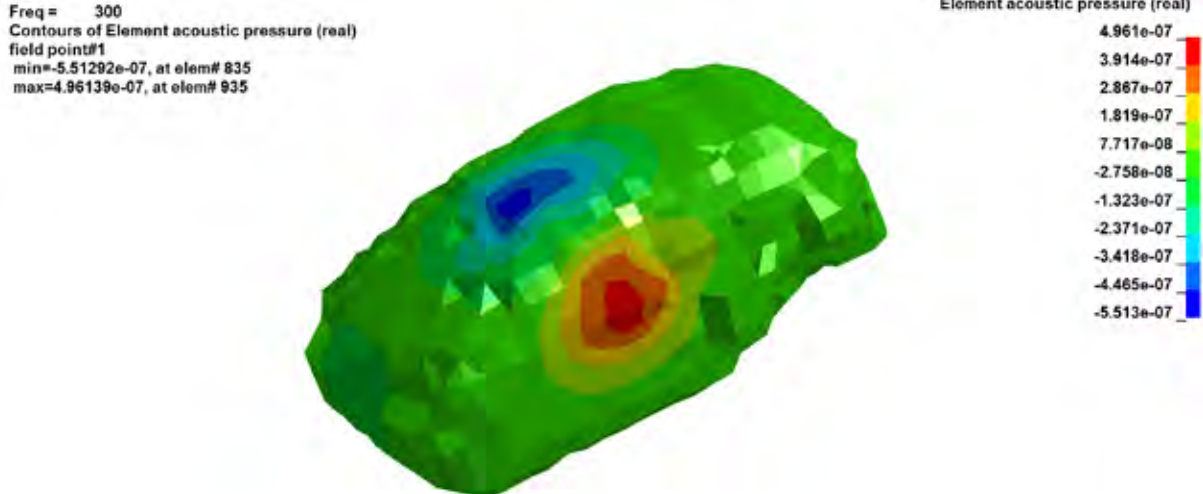

Figure 8. A simple car compartment BEM model

Figure 9. Real part of element acoustic pressure contribution for field point 100001 at 300 Hz
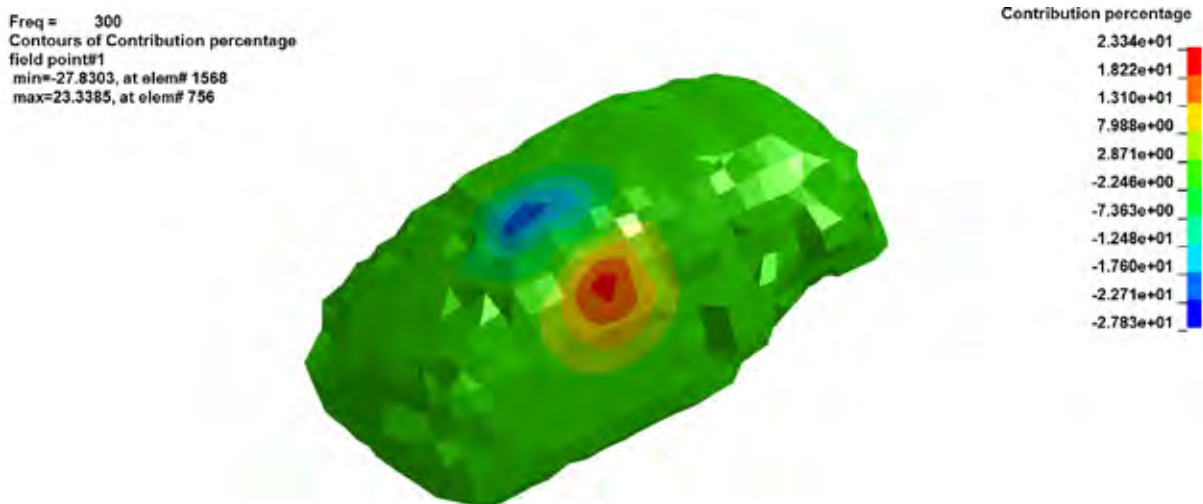

Figure 10. Element contribution percentages for acoustic pressure at field point 100001 at 300 Hz

2.4 D3ATV

The binary plot file D3ATV saves acoustic transfer vector results. The analysis is activated by the keyword ***FREQUENCY_DOMAIN_ACOUSTIC_BEM_ATV**.

ATV provides the acoustic pressure at field points due to unit normal velocity at each of the nodes (or elements) composing the acoustic domain surface. For each field point, for each frequency, the ATV is a complex vector with N components, where N is the total number of nodes (or elements) in acoustic boundary elements. D3ATV saves the real and imaginary parts of the complex pressure, and the sound pressure level (dB).

ATV is defined as the transfer function between the normal nodal (or elemental) velocity and the acoustic pressure at field points. Once all the ATV vectors are obtained, the total acoustic pressure at field points can be computed by a simple matrix – vector multiplication, as in equation (3),

$$\begin{Bmatrix} p_1 \\ p_2 \\ \vdots \\ p_i \\ \vdots \\ p_m \end{Bmatrix} = \begin{bmatrix} W_{1,1} & W_{1,2} & \cdots & W_{1,j} & \cdots & W_{1,n} \\ W_{2,1} & W_{2,2} & \cdots & W_{2,j} & \cdots & W_{2,n} \\ \vdots & \vdots & \ddots & \vdots & \ddots & \vdots \\ W_{i,1} & W_{i,2} & \cdots & W_{i,j} & \cdots & W_{i,n} \\ \vdots & \vdots & \ddots & \vdots & \ddots & \vdots \\ W_{m,1} & W_{m,2} & \cdots & W_{m,j} & \cdots & W_{m,n} \end{bmatrix}_{m' n} \begin{Bmatrix} v_1 \\ v_2 \\ \vdots \\ v_j \\ \vdots \\ v_n \end{Bmatrix}$$

(3)

or equation (4) in short form

$$\{P\}_m = [ATV]_{m' n} \{v\}_n$$

(4)

In equation (3), p_i is the acoustic pressure at field point i and v_j is the actual normal velocity at node j. m is the number of field points and n is the number of nodes (or elements) in boundary elements. $\Omega_{i,j}$ represents the acoustic pressure at field point i, due to unit normal velocity at node (or element) j. Please note that all the variables in equations (3) and (4) are dependent on round frequency $w = 2p\ f$. Besides, the variables in both equations are complex.

As indicated by equation (4), for a given frequency and given geometry, the ATV matrix is constant and is not dependent on the loading condition. Once the ATV matrix is obtained, for any given normal velocity vector $\{v\}_n$, a simple matrix-vector multiplication can provide the total pressure $\{P\}_m$ quickly. That is why this method is very efficient and provides huge saving in CPU times if multiple loading cases have to be considered.
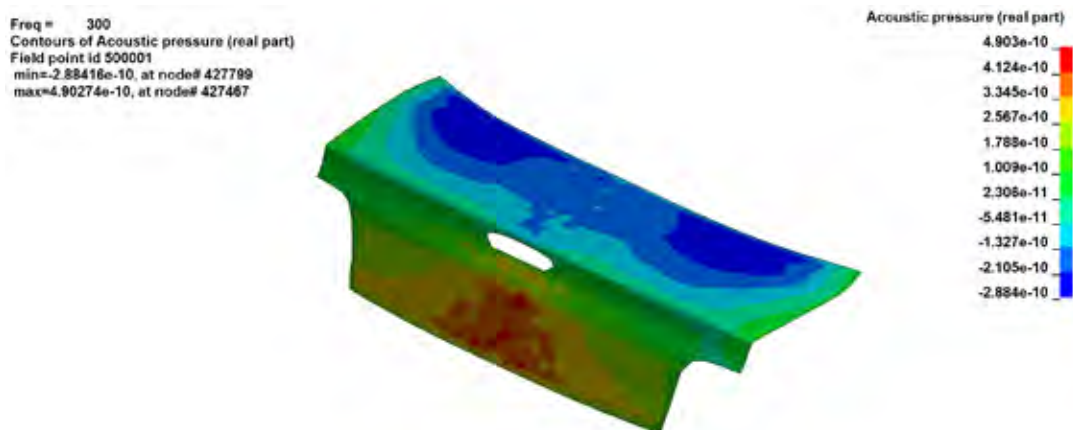

Figure 11. A trunk lid BEM model

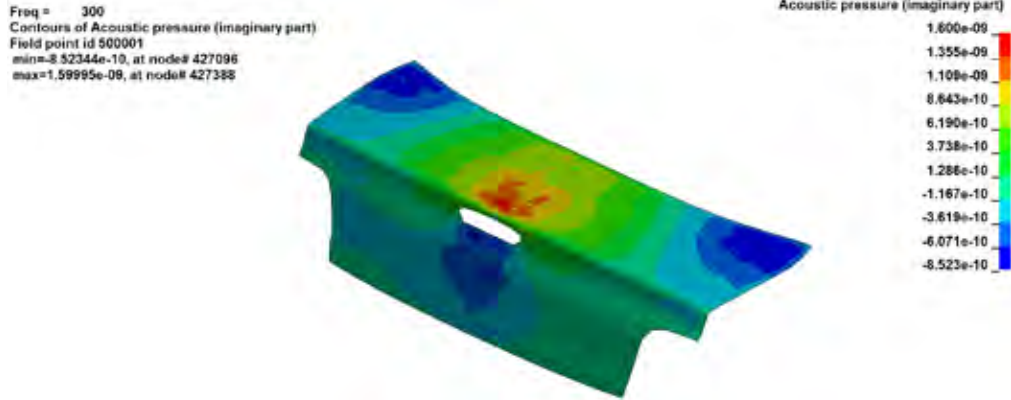Figure 12. Real part of pressures ATV at point 500001

Figure 13. Imaginary part of pressure ATV at point 500001

A trunk lid model is used to illustrate the D3ATV database (figure 11). Figures 12 and 13 show the real and imaginary part of pressure ATV at point 500001.

2.5 D3ERP

The binary plot file D3ERP saves ERP (equivalent radiated power) analysis results. The analysis is activated by the keyword ***FREQUENCY_DOMAIN_SSD_ERP**.

The ERP calculation is based on plane wave assumption for the radiated acoustic waves. First we calculate the ERP density, which is defined as

$$ERP_r = \frac{1}{2} r \, c \, \mathrm{Re}[v_n \times \overline{v}_n] \tag{5}$$

Where r is the density of acoustic medium, c is the sound speed and v_n is the normal velocity on the surface of the structure.

The ERP absolute value radiated from the vibrating panels is the integral of the ERP density over the whole surface and is given by

$$ERP_{abs} = \oint_S ERP_r \, dS = \frac{1}{2} r \, c \oint_S \mathrm{Re}[v_n \times \overline{v}_n] dS \tag{6}$$

It can be converted to a dB value if a reference value ERP_{ref} is provided.

$$ERP_{dB} = 10\log_{10}\left(ERP_{abs} / ERP_{ref}\right) \tag{7}$$

A simplified engine model is used to illustrate the D3ERP database (figure 14). The whole surface of the engine is defined as sound radiating panel, by a set of segments (***SET_SEGMENT**). Figure 15 shows the ERP density at frequency 100Hz.
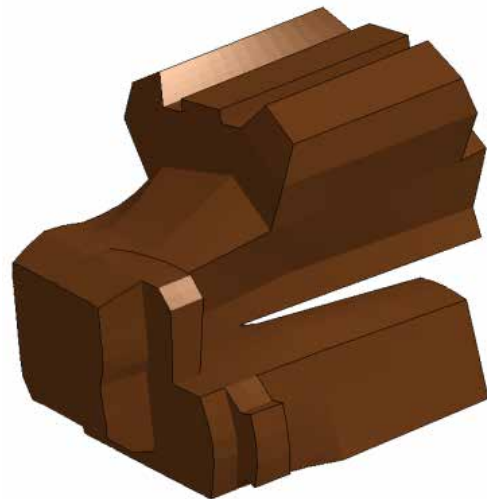

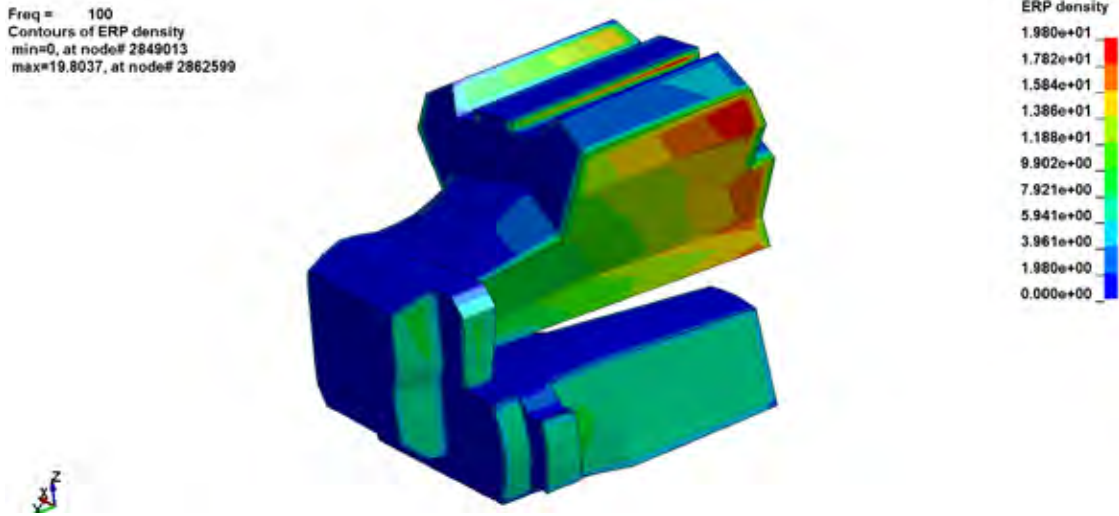Figure 14. A simplified engine BEM model

Figure 15. ERP density plot at frequency 100 Hz

2.6 D3EIGV_AC

The binary plot file D3EIGV_AC saves acoustic eigen frequencies and eigen vectors. The analysis is activated by the keyword ***FREQUENCY_DOMAIN_ACOUSTIC_FEM_EIGENVALUE**. The acoustic eigen vector is an array of acoustic pressure given at the nodes in the acoustic volume. Each node has one scalar acoustic pressure.

The acoustic eigenvalue analysis not only provides valuable characteristic information on the acoustic system itself, but also provides basis for modal solution method (comparing to direct solution method) for large scale problems.

An auto compartment model is used to illustrate the D3EIGV_AC database (figure 16). For acoustic eigenvalue analysis in LS-DYNA, various types of constraints on the boundary can be considered, like the prescribed pressure boundary condition. Figure 17 shows acoustic eigenvector for the 2nd mode. For this example, since no constraints are applied, the 1st mode is rigid body mode.

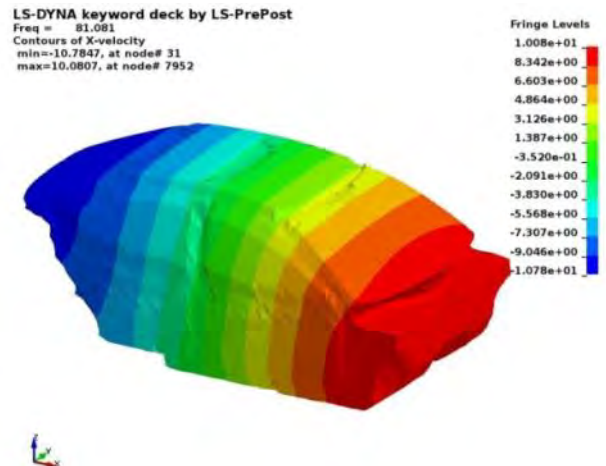Figure 16. An auto compartment FEM model   Figure 17. Acoustic eigenvector for the 2nd mode

Table 1 gives a summary of the acoustic binary databases, with their purpose and associated activating keywords in LS-DYNA.

Table 1. Acoustic binary databases

File name	Purpose	Activated by
D3ACS	Acoustic pressure on surface by BEM, in volume including surface by FEM	***DATABASE_FREQUENCY_BINARY_D3ACS** by BEM or FEM
D3ACP	Acoustic pressure plot	***FREQUENCY_DOMAIN_ACOUSTIC_FRINGE_PLOT** by BEM
D3ACC	Acoustic element contribution plot	***DATABASE_FREQUENCY_BINARY_D3ACC** by BEM
D3ATV	Acoustic transfer vector	***FREQUENCY_DOMAIN_ACOUSTIC_BEM_ATV**
D3ERP	Equivalent radiated power plot	***FREQUENCY_DOMAIN_SSD_ERP**
D3EIGV_AC	Acoustic eigen vector	***FREQUENCY_DOMAIN_ACOUSTIC_FEM_EIGENVALUE**

3. ASCII database for XY plot

Many ASCII databases have been provided in LS-DYNA's BEM and FEM acoustic solvers. The default acoustic ASCII databases are Press_Pa and Press_dB for both BEM and FEM acoustic solvers. The Sound Pressure is the force (N) of sound on a surface area (m^2) perpendicular to the direction of the sound. The SI-units for the sound pressure are N/m^2 or Pa. Sound pressure level (SPL) is a logarithmic measure of the effective pressure of a sound relative to a reference value. Sound Pressure Level can be expressed as (8)

$$L_p = 20\log_{10}\left(P/P_{ref}\right)$$
(8)

Where L_p is the sound pressure level (dB), P is the sound pressure (Pa) and P_{ref} is a reference pressure. Usually, in International Unit System the reference pressure is 2×10^{-5} Pa.

If the IPFILE is equal to 1 in BEM or FEM keywords, the real and imagniary parts of the sound pressure are output to ASCII files Press_Pa_real and Press_Pa_imag as the sound pressure is a complex variable.

If the TRSLT is great than zero in BEM, the time domain data of sound pressue and sound pressure level are calculated using inverse FFT and output to ASCII files Press_Pa_t and Press_dB_t.

Sound power or acoustic power is the rate at which sound energy is emitted, reflected, transmitted or received, per unit time. The SI unit of sound power is the watt(W). It is the power of the sound force on a surface of the medium of propagation of the sound wave. For a sound source, unlike sound pressure, sound power is neither room-dependent nor distance-dependent. Sound pressure is a measurement at a point in space near the source, while the sound power of a source is the total power emitted by that source in all directions. It is calculated by collocation BEM (methods 3 and 4) and output to Press_Power.

The radiation efficiency indicates how much sound power W a given structure radiates compared with the vibrating infinite flat surface for the same area. The radiation efficiency is thus given by equaltion (9). In general, the radiation efficiency is low meaning that structural vibrations have difficulty to produce noise. It is calculated by collocation BEM (methods 3 and 4) and output to Press_radef.

$$s = \frac{W}{\frac{1}{2}\,rcS\left\langle |v|^2 \right\rangle}$$
(9)

where $\langle ... \rangle$ denotes a spatial average and v is the amplitude of the velocity normal to the surface of the structure.

User can also request calculation for weighted sound pressure level A,B,C and D by setting different value of DBA in BEM or FEM. Below is the information about weighted sound pressure level [3].

·   A-weighting: the A-weighting filter covers the full audio range - 20 Hz to 20 kHz and the shape is similar to the response of the human ear at the lower levels - see the equal loudness contours entry. A-weighted noise measurements are widely used and the meter class confirms the accuracy of the meter including the filters. A weighted measurements correlate well with the perceived loudness at low sound levels, as originally intended. However the current use for most noise applications, supported by regulations, does cause concern in some quarters.

·   B-weighting: no longer in common use, was initially developed to cover the mid-range between the A and C-weighting networks. It was also more 'critical' of lower frequencies than the A-weighting network which probably accounts for its use by the motor industry for many years after its general decline in popularity.

·   C-weighting: a standard frequency weighting for sound level meters, commonly used for higher level measurements and peak - sound pressure levels. The A-weighting curve is used extensively for general purpose noise measurements but the C-weighting correlates better with the human response to high noise levels.

·   D-weighting: sound level meter frequency weighting developed for measuring aircraft noise especially non-bypass military engines. It is not in common use since IEC 61672 2003. More recent ISO standards recommend A-weighting for commercial aircraft noise.

A simple compartment FEM model is used to show the weighted sound pressure level (figure 3). Figure 18 shows the normal SPL and weighted SPL at field point 8106.
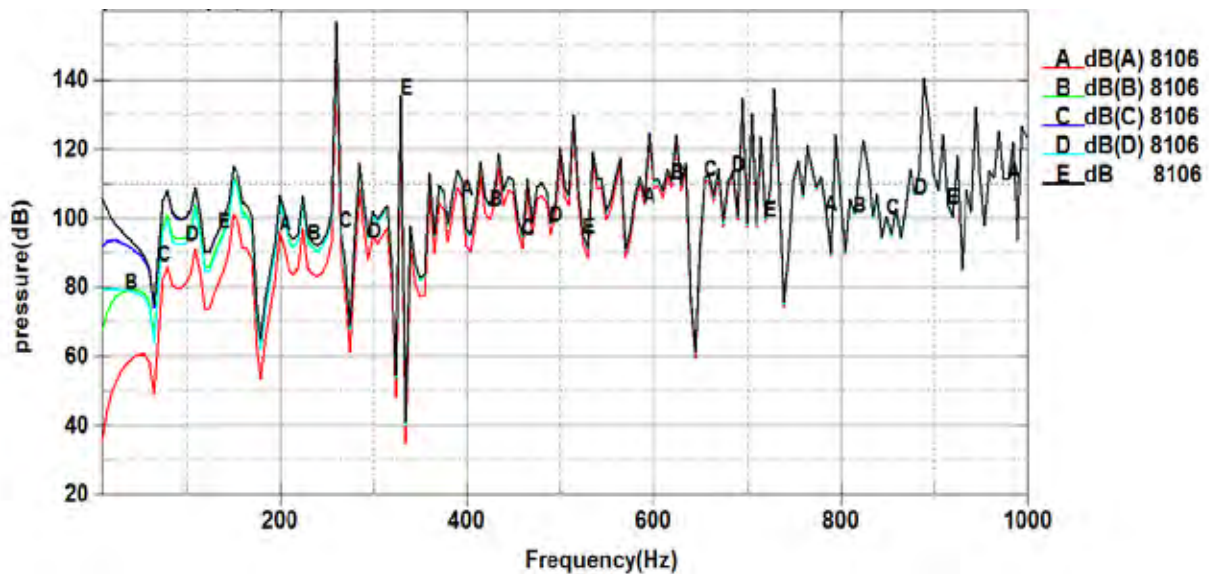

Figure 18. Normal SPL and weighted SPL at point 8106

Panel contribution analysis is conducted to identify the panels which have a high contribution on the acoustic response. It gives the contribution percentage of panels (given as part, set of parts or set of segments) on the acoustic results at observation points and output to ASCII file Panel_contribution_NID.

A simplified tunnel model is employed to illustrate the panel contribution analysis. The model is shown in figure 19. Figure 20 shows the panel contribution percentage of the four panels respectively. One can see that

the top panel (panel 3) makes the largest contribution for the noise for most frequencies. The contribution from panel 1 and panel 2 are almost identical due to the symmetry of the structure.
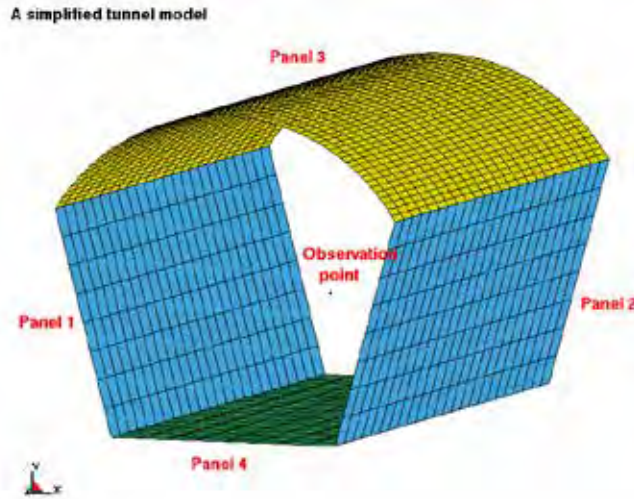

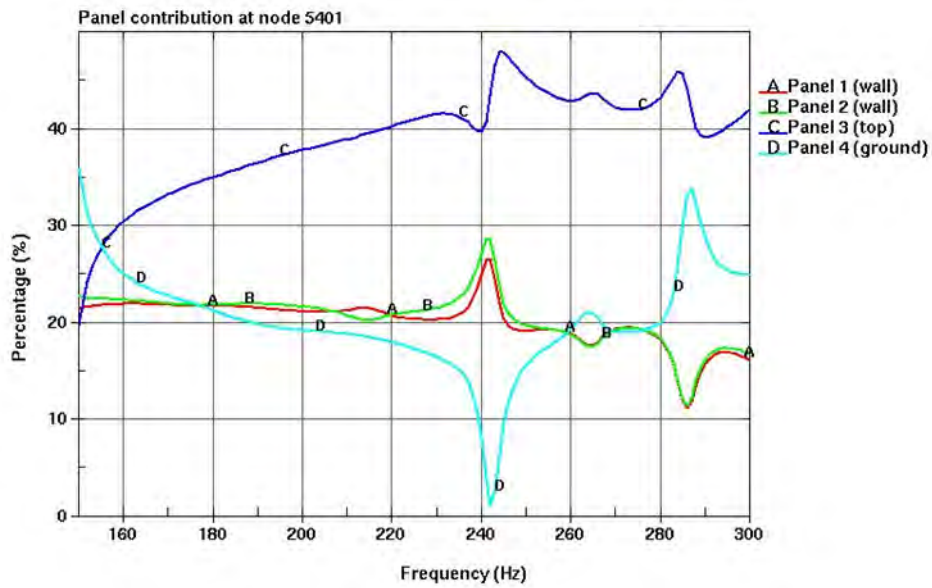Figure 19. A simplified tunnel BEM model

Figure 20. Different panel contributions at point 5401

Table 2 gives a summary of the acoustic ASCII databases, with their purpose and associated activating keyword in LS-DYNA.

Table 2. Acoustic ASCII databases

File name	Purpose	Activated by
Press_Pa	Pressure (abs) vs. Freq	BEM or FEM
Press_dB	SPL (dB) vs. Freq	BEM or FEM

Press_Pa_real	Pressure (real) vs. Freq	IPFILE=1 by BEM or FEM
Press_Pa_imag	Pressure (imag) vs. Freq	IPFILE=1 by BEM or FEM
Press_Pa_t	Pressure (abs) vs. Time	TRSLT>0 by BEM
Press_dB_t	SPL (dB) vs. Time	TRSLT>0 by BEM
Press_Power	Sound Power vs. Freq	BEM Method = 3 or 4
Press_radef	Radiation efficiency vs. Freq	BEM Method = 3 or 4
Press_dB(A)	SPL (dB, A-weighting) vs. Freq	dBA=1 in BEM or FEM
Press_dB(B)	SPL (dB, B-weighting) vs. Freq	dBA=2 in BEM or FEM
Press_dB(C)	SPL (dB, C-weighting) vs. Freq	dBA=3 in BEM or FEM
Press_dB(D)	SPL (dB, D-weighting) vs. Freq	dBA=4 in BEM or FEM
Panel_contribution_NID	Panel contribution vs. Freq	Option: **PANEL_CONTRIBUTION** by BEM

4. Summary

The paper gives a review of the acoustic databases, which have different purposes and should be used in different circumstances. Users may get confused with these variety of binary and ASCII databases. With this paper, we give a detailed review of these acoustic databases, and explain the difference among them. Some examples are provided to demonstrate the application of these databases.

Some of the databases were implemented to answer the request from users or under the suggestion from users. The authors are grateful to the users for their suggestions and feedback.

References

[1] Livermore Software Technology Corporation: "LS-DYNA Keyword User's Manual", 2016

[2] F. J. Fahy and P. Gardonio, Sound and Structural Vibration: Radiation, Transmission and Response. Academic Press, London, 2nd edition, 2006

[3] Source of information: http://www.acoustic-glossary.co.uk/frequency-weighting.htm